BaCu$_2$Si$_2$O$_7$: A quasi-one-dimensional $S=1/2$ antiferromagnetic chain system

I. Tsukada, Y. Sasago,* and K. Uchinokura
Department of Applied Physics, The University of Tokyo, 7-3-1 Hongo, Bunkyo-ku, Tokyo 113-8656, Japan

A. Zheludev, S. Maslov, and G. Shirane
Brookhaven National Laboratory, Upton, New York 11973-5000

K. Kakurai
Neutron Scattering Laboratory, Institute for Solid State Physics, The University of Tokyo, Tokai, Ibaraki 319-1106, Japan

E. Ressouche
MDN/SPSMS/DRFMC CEN Grenoble, 17 rue des Martyrs, 38054 Grenoble Cedex, France
(Received 16 February 1999)

The antiferromagnetic (AF) compound BaCu$_2$Si$_2$O$_7$ is studied by magnetic susceptibility and neutron-scattering techniques. The observed behavior is dominated by the presence of loosely coupled $S=1/2$ chains with the intrachain AF exchange constant $J_{\parallel} \approx 24.1$ meV. Long-range Néel ordering is observed below T_N $=9.2$ K. The results are discussed within the framework of the mean-field RPA model for weakly interacting quantum spin chains. [S0163-1829(99)03433-5]

I. INTRODUCTION

The amazing structural diversity of copper-oxide compounds makes these materials very useful as model systems for fundamental studies of low-dimensional magnetism. In most cases their unique properties result from the particular topologies of the corresponding spin networks formed by magnetic Cu^{2+} ions. Examples of such networks are found in CuGeO$_3$ (linear chain: spin-Peierls),[1] CaCuGe$_2$O$_6$ (isolated dimer),[2,3] BaCuSi$_2$O$_6$ (two-dimensional bilayer),[4] Sr$_2$CuO$_3$ (rigid linear chain),[5] SrCu$_2$O$_3$ (two-leg ladder),[6] and SrCuO$_2$ (edge-shared double linear chain),[7] etc. Magnetic interactions in all these systems are determined by the microscopic spatial coordination of Cu^{2+} and O^{2-}.[8] The so-called corner-sharing ($\angle$Cu-O-Cu$\approx 180°$) and edge-sharing ($\angle$Cu-O-Cu$\approx 90°$) configurations have been extensively studied. A far richer spectrum of properties is expected from systems with intermediate bond angles, and the search for realizations of such coupling geometries has become important.

The rather poorly studied BaCu$_2$Si$_2$O$_7$ is a good example of a zigzag chain network of corner-sharing CuO$_4$ plaquettes (Fig. 1) with intermediate values of $\angle$Cu-O-Cu bond angles, 124°. The crystal structure is orthorhombic, space group *Pnma*, with the cell constants being $a=6.862(2)$ Å, $b=13.178(1)$ Å, and $c=6.897(1)$ Å.[9] The spin chains run along the c crystallographic axis. In the present paper we report magnetic susceptibility measurements and inelastic neutron-scattering experiments on this material. We find it to be an excellent model of weakly coupled quantum $S=1/2$ chains, exhibiting a crossover from one-dimensional (1D) behavior at high temperatures to 3D behavior and long-range antiferromagnetic (AF) (Néel) order at low temperatures. As anticipated for a system with intermediate values of bond angles, the magnetic properties are extremely sensitive to slight modifications in atomic positions. This is demonstrated by preliminary susceptibility results for BaCu$_2$Ge$_2$O$_7$, which, unlike the isomorphous BaCu$_2$Si$_2$O$_7$, orders in a weak-ferromagnetic structure with a small net magnetization.

II. EXPERIMENTAL

Polycrystalline samples of BaCu$_2$Si$_2$O$_7$ (or BaCu$_2$Ge$_2$O$_7$) were prepared by conventional solid-state reaction method, using BaCO$_3$, SiO$_2$ (or GeO$_2$), and CuO as starting materials. The polycrystalline rods were crushed to fine powder for neutron powder diffraction studies. Single crystals were grown using the floating-zone technique from a sintered polycrystalline rod. In inelastic neutron-scattering experiments we utilized an as-grown single-crystal rod (5 mm diameter $\times$ 10 mm long). A small fragment cut to a 3-mm^3 cube was used in single-crystal susceptibility measurement.
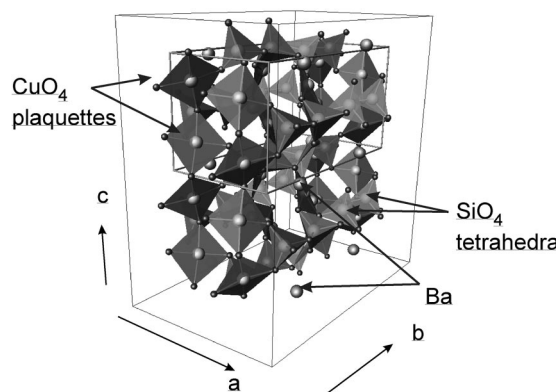

FIG. 1. A schematic view of the crystal structure of BaCu$_2$Si$_2$O$_7$. Chains of corner-sharing CuO$_4$ plaquettes run along the c crystallographic axis and are supported by a network of SiO$_4$ tetrahedra.

All magnetic susceptibility experiments were done with a commercial superconducting quantum interference device magnetometer (χ-MAG7, Conductus Co., Ltd.) in the temperature range of 2–300 K. Neutron powder diffraction experiments were carried out at the 400 cells CRG diffractometer D1B at Institut Laue Langevin (Grenoble, France). Single-crystal neutron-scattering studies were performed with the ISSP-PONTA triple-axis spectrometer at 5G beam hole at the Japan Research Reactor 3M at the Japan Atomic Energy Research Institute (Tokai, Japan). Pyrolytic graphite PG(002) reflections were used in the monochromator and analyzer. The collimation setup was $60'$-$80'$-$40'$-$80'$, with a PG filter positioned after the sample. The final neutron energy was fixed at $E_f = 14.7$ meV. The sample was mounted in a standard ''ILL Orange'' cryostat with the $(0,k,l)$ reciprocal-space plane in the scattering plane of the spectrometer, and the data were collected in the temperature range 2–15 K.

III. RESULTS

A. Magnetic susceptibility

The temperature dependences of dc magnetic susceptibility measured under $H = 10$ kOe in $BaCu_2Si_2O_7$ and $BaCu_2Ge_2O_7$ are shown in Fig. 2(a). The experimental curve for $BaCu_2Si_2O_7$ shows a sharp peak around 9 K and a broad maximum around 150 K. The $BaCu_2Si_2O_7$ data were fit to the theoretical Bonner-Fisher (BF) curve for a one-dimensional $S = 1/2$ quantum antiferromagnet[10] (solid lines). A Heisenberg exchange constant $J \approx 280$ K (24.1 meV) was obtained from this analysis.[11] Note that the BF fit becomes rather poor in the low-temperature region, suggesting the onset of three-dimensional spin correlations in this regime.

To identify the low-temperature ordered structure of $BaCu_2Si_2O_7$ below 9.2 K, the anisotropy of magnetic susceptibility was studied in a single-crystal sample. The measured temperature dependences are shown in Fig. 2(b). Signs of long-range Néel ordering are clearly seen. Below 9.2 K a substantial drop is observed in χ_c, while both χ_a and χ_b change little from 9.2 K down to 2 K. This clearly points to the presence of antiferromagnetic long-range order below $T_N = 9.2$ K with crystallographic c axis being the magnetic easy axis of the system. Note that at $T \to 0$ χ_c retains a substantial nonzero value, suggesting a reduction of ordered moment, presumably due to the 1D nature of the system. As expected, the one-dimensional character of paramagnetic phase is observed in single crystals as well. The susceptibility shows broad maxima around 180 K along all the three crystallographic directions. Fitting these data to a BF curve, and assuming an anisotropic g factor, we obtain $g_a = 2.5$ and $g_b = g_c = 2.2$.

For $BaCu_2Ge_2O_7$ a BF analysis [dashed line in Fig. 2(a)] of the high-T part of the experimental $\chi(T)$ curve yields $J \approx 540$ K (46.5 meV), i.e., much larger than for $BaCu_2Si_2O_7$. In the low-temperature region the magnetic susceptibilities of the two isomorphous compounds become qualitatively different. The drastic increase of magnetization in $BaCu_2Ge_2O_7$ observed below 8.5 K is attributed to the appearance of uniform spontaneous magnetization. This increase is particularly well seen in the low-field measurement [Fig. 2(a), inset]. The saturation value of magnetization
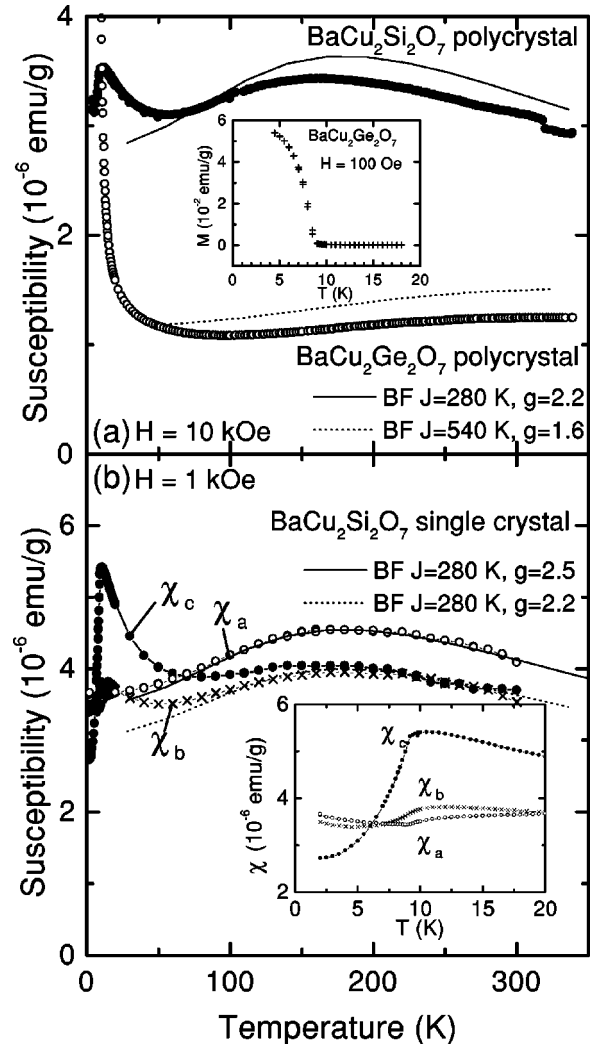

FIG. 2. (a) Magnetic susceptibility of polycrystalline samples of $BaCu_2Ge_2O_7$ and $BaCu_2Si_2O_7$ measured at $H = 10$ kOe. Solid and dotted lines are fits to the theoretical Bonner-Fisher curve. The inset shows an evolution of magnetization in $BaCu_2Ge_2O_7$, measured in a weak magnetic field of 100 Oe. (b) Magnetic susceptibility of single-crystal $BaCu_2Si_2O_7$ measured in $H = 1$ kOe magnetic field applied along the principal axes. Solid and dotted lines are as in (a). The inset shows magnified curves around T_N.

($\approx 6 \times 10^{-2}$ emu/g) is orders of magnitude less than 22.15 emu/g, that one would obtain if all the Cu^{2+} spins were aligned ferromagnetically. The clear dominance of c-axis antiferromagnetism in the paramagnetic phase of $BaCu_2Ge_2O_7$ suggests that the spontaneous uniform moment below 8.5 K is a result of a canted weak-ferromagnetic spin arrangement.

B. Neutron diffraction

As a first step towards determining the magnetic structure of $BaCu_2Si_2O_7$ we performed neutron powder diffraction experiments at 2 and 15 K, i.e., above and below the Néel temperature. Subtraction of the powder scan data collected at these two temperatures did not reveal any sign of magnetic Bragg reflections. This failure to observe any magnetic signal in the powder experiment can be attributed to a small value of ordered moment and the fact that all magnetic reflections appear on top of strong nuclear peaks (see below),
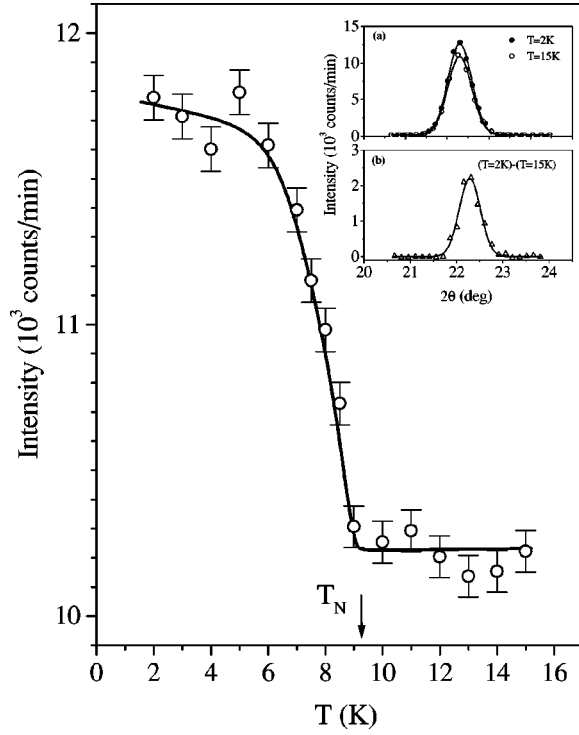
FIG. 3. Inset: (a) Elastic $\theta-2\theta$ neutron scans through the (011) Bragg reflection collected above and below the magnetic ordering temperature in BaCu₂Si₂O₇. (b) The corresponding magnetic contribution obtained by subtracting the data shown in (a). Main panel: measured temperature dependence of the (011) peak intensity. Below $T_N=9.2$ K the magnetic Bragg peak emerges on top of the (011) nuclear reflection.

FIG. 4. Constant-energy scan measured at $T=2$ K in BaCu₂Si₂O₇, for energy transfers (a) $\hbar\omega=10$ meV along the (0, -1.5, l) direction, and (b) $\hbar\omega=5$ meV along the (0, 0, l) direction. Solid lines are theoretical fits as described in the text.

not surprising for a structure with eight magnetic Cu²⁺ ions per unit cell, and are thus very difficult to detect.

Even in the subsequent single-crystal experiment, only limited information on the magnetic structure of AF phase of BaCu₂Si₂O₇ could be obtained. Only one magnetic reflection, namely (011), could be reliably measured at low temperatures. The (011) *nuclear* reflection is allowed by crystal symmetry, but its intensity is fortunately relatively weak. The inset (a) in Fig. 3 shows rocking curves of the (011) Bragg peak measured above (open circles) and below (solid circles) the magnetic transition temperature. The difference between these two scans is shown in the inset (b) of Fig. 3. The measured peak intensity is plotted against temperature in the main panel of Fig. 3. The observed increase upon cooling through $T_N=9.2$ K is attributed to long-range magnetic ordering. Intensities of several other Bragg peaks, including (031), (013), (051), (071), (053), and (035) were also measured as functions of temperature. However, the nuclear contribution to these reflections is much larger than that for (011), and no intensity increase could be observed beyond the experimental error bars upon cooling through T_N.

C. Inelastic scattering

Inelastic neutron-scattering studies of spin excitations in BaCu₂Si₂O₇ were also performed. The rather steep spin-wave dispersion along the chain axis was measured in two constant-E scans near the 1D AF zone center $\vec{Q}=(0, -1.5, l)$, at energy transfers $\hbar\omega=10$ meV [Fig. 4(a)] and
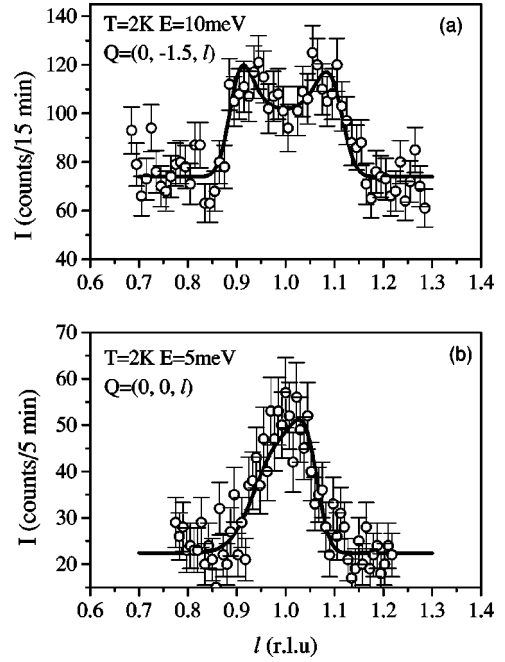
$\vec{Q}=(0,0,l)$ at $\hbar\omega=5$ meV [Fig. 4(b)]. Both data sets were collected at $T=2$ K, and transverse wave vector k was chosen to optimize focusing conditions. Even in the 10-meV scan the two spin-wave branches are barely resolved. Unfortunately, for higher energy transfers the magnetic signal was too weak to be measured in the present experiment.

The spin-wave dispersion along the b axis was measured at $T=2$ K in constant-Q scans at three reciprocal-space points at the bottom of longitudinal dispersion (Fig. 5): $\vec{Q}=(0,0,1)$, $\vec{Q}=(0,0.5,1)$, and $\vec{Q}=(0,1.1,1)$. Clearly the transverse bandwidth (≈ 1 meV) is very small compared to that along the chain axis, which confirms the 1D character of spin correlations in BaCu₂Si₂O₇. Even in the vicinity of the 3D magnetic zone center (011) the excitation energy appears to extrapolate to a nonzero value, i.e., the spectrum has a gap $\Delta_{(011)}\approx 1.5$ meV.

IV. DISCUSSION

All our experimental results point to that both BaCu₂Si₂O₇ and BaCu₂Ge₂O₇ should be considered as quasi-1D systems, dominated by strong intrachain antiferromagnetic exchange interactions. Long-range ordering at low temperatures occurs owing to a much weaker interchain coupling. The subtleties of the low-temperature magnetic structures and magnetic anisotropy, as well as the variations of the intrachain coupling constant J in the two systems are expected to be related to the details of the microscopic atomic arrangement.

A. Microscopic structure and magnetic interactions

Rather remarkable is the drastic (a factor of 2) difference in the intrachain AF exchange constants of the two isomor-
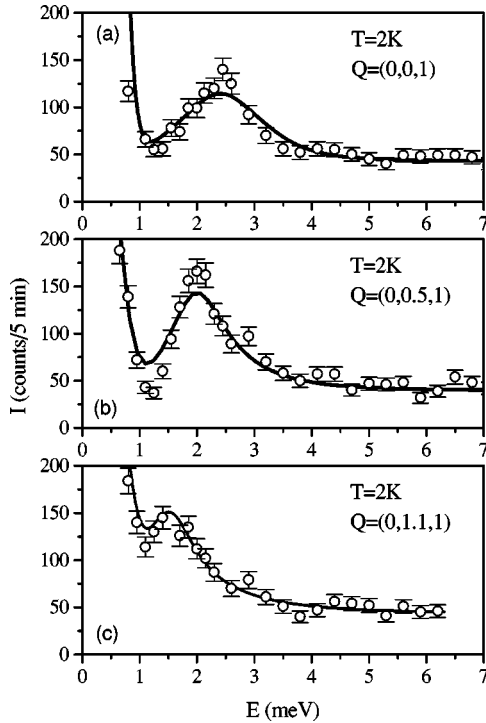
FIG. 5. Constant-Q scans measured in BaCu$_2$Si$_2$O$_7$ at $T = 2$ K. (a) $\mathbf{Q} = (0,0,1)$, (b) $\mathbf{Q} = (0,0.5,1)$, and (c) $= (0,1.1,1)$. Solid lines are single-mode approximation fits, as described in the text.

phous systems BaCu$_2$Si$_2$O$_7$ and BaCu$_2$Ge$_2$O$_7$. The AF spin chains in these species are formed by corner-sharing CuO$_4$ plaquettes, and the main contribution to AF interactions is expected to be the standard superexchange mechanism involving the shared O sites. A single chain is visualized in Fig. 6(a). Only the Cu sites and the shared oxygen sites are shown. The Cu^{2+} ions are almost perfectly lined up. However, the Cu-O-Cu bond angle is substantially smaller than
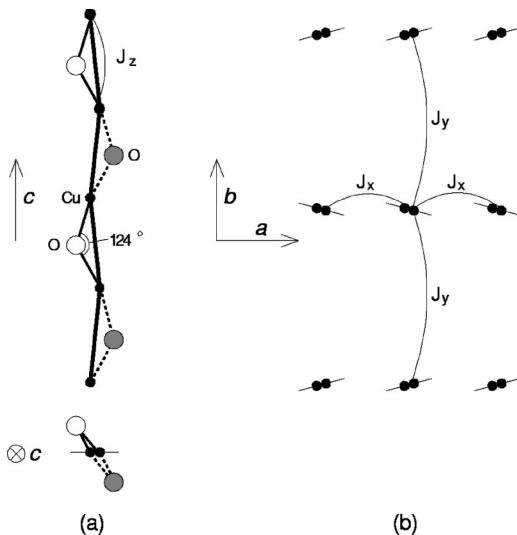

FIG. 6. A schematic representation of the magnetic ion arrangement in BaCu$_2$Si$_2$O$_7$. (a) A single Cu-O chain. Cu-O-Cu bond angles are shown explicitly. (b) Relative arrangement of individual chains, projected onto the (ab) crystallographic plane. Interchain interactions are characterized by two nearest-neighbor exchange constants J_x and J_y.

180°. The difference in J is most likely due to a difference in this crucial bonding angle: 124° in BaCu$_2$Si$_2$O$_7$ and 135° in the Ge-based system.[9] Indeed we know that a larger bond angle is more favorable for superexchange involving oxygen.

Subtle structural differences between the two systems are also to be held responsible for the difference in the low-T behavior. In addition to single-ion anisotropy that manifests itself in the anisotropy of the g factor and the gap in the spin-wave spectrum (see discussion below), one should also consider the possibility of Dzyaloshinskii-Moriya (DM) asymmetric exchange interaction. The latter is allowed by local Cu-site symmetry in BaCu$_2$Si$_2$O$_7$ and BaCu$_2$Ge$_2$O$_7$, and may be responsible for the weak ferromagnetism of BaCu$_2$Ge$_2$O$_7$. The correlation between the microscopic structure and magnetic properties of BaCu$_2$Si$_2$O$_7$ and BaCu$_2$Ge$_2$O$_7$ is indeed a very interesting problem. However, at the present stage we do not have sufficient information required for a more detailed discussion of this subject, and suggest that further experiments, possibly using polarized neutron diffraction, should be performed to clarify the magnetic structures in the ordered state.

B. Weakly coupled quantum spin chains

Ignoring for now such subtleties as magnetic anisotropy, spin canting in the ordered state and the possibility of DM interaction, we shall turn to discussing what makes the two systems really valuable for our cause, namely the 1D quantum antiferromagnetic aspect of their magnetic properties. In the following sections we shall demonstrate that the observed behavior of BaCu$_2$Si$_2$O$_7$ can be very well understood within the framework of existing theories for weakly coupled $S = 1/2$ AF chains. Particularly useful for describing such systems are the chain-MF (mean field)[12–14] and the corresponding chain-RPA (random phase approximation) models.[14,15] These approaches were previously shown to work extremely well for a number of well-characterized compounds (see for example Refs. 16,17, and references therein).

1. A model Hamiltonian

Before we can apply these MF-RPA theories to our particular system, we have to construct a model spin Hamiltonian for BaCu$_2$Si$_2$O$_7$. A slight complication arises from a non-Bravais arrangement of magnetic ions in the crystal. Indeed, the fractional cell coordinates of Cu^{2+} are (i) $(0.25 - \delta_x, \delta_y, 0.75 + \delta_z)$, (ii) $(0.25 + \delta_x, -\delta_y, 0.25 + \delta_z)$, (iii) $(0.75 - \delta_x, 0.5 - \delta_y, 0.75 - \delta_z)$, (iv) $(0.75 + \delta_x, 0.5 + \delta_y, 0.25 - \delta_z)$, (v) $(0.75 + \delta_x, -\delta_y, 0.25 - \delta_z)$, (vi) $(0.75 - \delta_x, \delta_y, 0.75 - \delta_z)$, (vii) $(0.25 + \delta_x, 0.5 + \delta_y, 0.25 + \delta_z)$, and (viii) $(0.25 - \delta_x, 0.5 - \delta_y, 0.75 + \delta_z)$, where $\delta_x = 0.028$, $\delta_y = 0.004$, and $\delta_z = 0.044$. The shifts δ_x and δ_z present few problems, as they do not disturb the equivalence of nearest-neighbor Cu-Cu bonds along the a and c axes, respectively. δ_y, on the other hand, leads to alternating nearest-neighbor Cu-Cu distances along the b axis. At present we shall ignore this slight alternation, assuming $\delta_y \approx 0$ and postulating nearest-neighbor Cu-Cu bonds to be equivalent along the b axis as well. The simplest nearest-neighbor Heisenberg Hamiltonian can then be written as

$$\hat{H} = \sum_{m,n,p} \mathbf{S}_{m,n,p}[J_x\mathbf{S}_{m+1,n,p} + J_y\mathbf{S}_{m,n+1,p} + J_z\mathbf{S}_{m,n,p+1}].$$
$$(1)$$

Here m, n, and p enumerate the spins $\mathbf{S}_{m,n,p}$ along the a, b, and c axes, respectively. As BaCu$_2$Si$_2$O$_7$ is clearly a quasi-1D antiferromagnet, $J_z > 0$ and $|J_z| \gg |J_y|, |J_x|$.

2. Reduction of ordered moment

One of the most important predictions of the chain-MF model is the relation between ordering temperature, magnitude of interchain coupling, and saturation moment at $T \rightarrow 0$. At the MF level the actual signs of magnetic interactions are not important and these properties are determined by the mean interchain coupling constant $|J_\perp| = (|J_x| + |J_y|)/2$. Schulz gives the relation between m_0, T_N, and $|J_\perp|$:[14]

$$|J_\perp| = \frac{T_N}{1.28\sqrt{\ln(5.8J/T_N)}}, \qquad (2)$$

$$m_0 \approx 1.017\sqrt{\frac{|J_\perp|}{J}}. \qquad (3)$$

In our case of BaCu$_2$Si$_2$O$_7$ the susceptibility data ($T_N = 0.793$ meV and $J = 24.1$ meV) gives $m_0 = 0.11\mu_B$.

To test this theoretical prediction we have to determine the spin structure in the ordered state. Unfortunately, with only one measured magnetic reflection we can only speculate on this. Let us consider an approximate collinear magnetic state, with all spins strictly along (001), as suggested by $\chi(T)$ measurements. The two simplest possible AF structures (A and B) consistent with the presence of a substantial (011) magnetic peak are shown in Figs. 7(a) and 7(b). We can estimate the magnitude of saturation moment that would be required in structures A and B to produce a (011) magnetic peak of measured intensity. Comparing the measured magnetic intensity of (011) to that of two strong nuclear reflections (020) and (022), and making use of the known room-temperature crystal structure,[9] for the saturated moment m_0 of Cu^{2+} we get $m_0 = 0.16\mu_B$ and $m_0 = 0.55\mu_B$ for structures A and B, respectively. A simple calculation of nuclear and magnetic structure factors indicates that a magnetic moment as large as $0.55\mu_B$ would be easily detected in a powder experiment at (h, k, l-odd) positions. The lack of any clear magnetic signal in our powder data suggests that of the two proposed structures only structure A can be realized in BaCu$_2$Si$_2$O$_7$. For structure A the estimated ordered moment is in rather good agreement with the predictions of Eq. (3). We shall thus use structure A as a working assumption for the spin arrangement in BaCu$_2$Si$_2$O$_7$. For the Hamiltonian (1) to stabilize this type of ground state we will have to assume the exchange interactions to be ferromagnetic along the a axis ($J_x < 0$), and antiferromagnetic along the b axis ($J_y > 0$).

3. Spin dynamics

As is well known, for an *isolated* antiferromagnetic $S = 1/2$ chain the dynamic structure factor can be described as a two-spinon excitation continuum.[18] To a good approximation
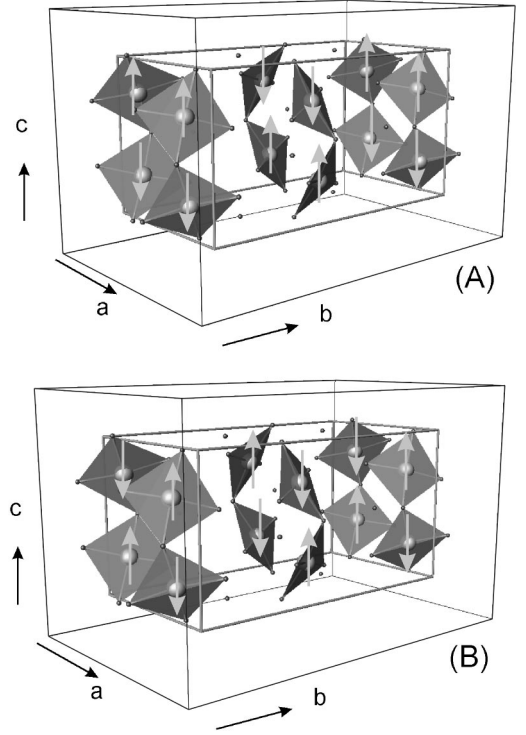

FIG. 7. Two simple collinear magnetic structures consistent with the available data on BaCu$_2$Si$_2$O$_7$, with ferromagnetic (A) and antiferromagnetic (B) nearest-neighbor coupling along the a axis.

$$S(q,\omega) \propto \frac{1}{\sqrt{\omega^2 - \omega_q^2}}\Theta(\omega - \omega_q), \qquad (4)$$

where ω_q is the lower bound of the continuum given by

$$\hbar\omega_q = \frac{\pi}{2}J_\parallel|\sin(q)|, \qquad (5)$$

and $J_\parallel$ is intrachain coupling constant. This type of behavior has been seen experimentally in a number of systems, in particular KCuF$_3$ (Refs. 16 and 19) and CuGeO$_3$ (Ref. 20). As mentioned above, spin correlations in *weakly coupled* quantum $S = 1/2$ spin chains are very well described by the chain-RPA model.[14,15] As the system becomes ordered in three dimensions, the spectrum develops a mass gap $\Delta(\vec{Q}_\perp)$ that depends on the transverse momentum transfer $\vec{Q}_\perp$. The bandwidth of transverse dispersion is of the order of $J_\perp$. This is in striking contrast with classical spin-wave theory, where the transverse bandwidth is proportional to $\sqrt{J_\perp J_\parallel}$. The mass gap goes to zero only at the 3D magnetic zone centers, i.e., at the position of magnetic Bragg reflections. A sharp single-magnon mode is the lowest-energy excitation that is split off from the lower bound of the continuum. A two-magnon continuum then starts at $2\Delta(\vec{Q}_\perp)$. The dispersion of the magnon branch is given by

$$(\hbar\omega_{\vec{Q}})^2 = \frac{\pi^2}{4}J_\parallel^2\sin^2(Q_\parallel) + \Delta^2(\vec{Q}_\perp). \qquad (6)$$

For the interchain coupling geometry of $KCuF_3$ (equal nearest-neighbor ferromagnetic interactions along the a and b axes) the expression for $\Delta(\vec{Q}_\perp)$ has been derived in Ref. 15.

Near the bottom of 1D dispersion the single mode approximation (SMA) works very well[14] and to a good approximation the dynamic structure factor at $T=0$ is given by

$$S(\vec{Q},\omega) \propto \frac{1}{\omega}\delta(\omega - \omega_{\vec{Q}}). \tag{7}$$

For $\hbar\omega \gg |J_x|, |J_y|$, on the other hand, it is more appropriate to use Eq. (4) for isolated chains.

The dynamic structure factor $S(\vec{Q},\omega)$ for the non-Bravais spin lattice in $BaCu_2Si_2O_7$ can be expressed through the dynamic structure factor $S_0(\vec{Q},\omega)$ of an equivalent system with the same exchange constants and a Bravais spin lattice. The latter is obtained by setting δ_x, δ_y, and δ_z to zero. It is straightforward to show that

$$\begin{aligned} S(\vec{Q},\omega) &= \cos^2(2\pi h\delta_x)\cos^2(2\pi l\delta_z)S_0(\vec{Q},\omega) \\ &+ \cos^2(2\pi h\delta_x)\sin^2(2\pi l\delta_z)S_0(\vec{Q}+\{001\},\omega) \\ &+ \sin^2(2\pi h\delta_x)\cos^2(2\pi l\delta_z)S_0(\vec{Q}+\{100\},\omega) \\ &+ \sin^2(2\pi h\delta_x)\sin^2(2\pi l\delta_z)S_0(\vec{Q}+\{101\},\omega). \end{aligned} \tag{8}$$

Here we have defined $Q = [(2\pi/a)h, (2\pi/b)k, (2\pi/c)l]$. In our particular case $\delta_x, \delta_z \ll 1$, so, for not too large momentum transfers $S(\vec{Q},\omega) \approx S_0(\vec{Q},\omega)$. In other words, we can safely analyze the measured inelastic scans assuming an idealized Bravais arrangement of Cu^{2+} sites.

We can now rewrite Eqs. (4) and (5) to match the notation introduced above for $BaCu_2Si_2O_7$:

$$S(\vec{Q},\omega) \propto \frac{1}{\sqrt{\omega^2 - \omega_{Q_\parallel}^2}}\Theta(\omega - \omega_{Q_\parallel}), \tag{9}$$

$$\hbar\omega_{Q_\parallel} = \frac{\pi}{2}J_z|\sin(\pi l)|. \tag{10}$$

The result for transverse dispersion $\Delta(\vec{Q}_\perp)$ derived for the case of $KCuF_3$ by Essler *et al.*[15] can also be easily adapted for use with the coupling geometry in $BaCu_2Si_2O_7$:

$$\begin{aligned} (\hbar\omega_{\vec{Q}})^2 &= \frac{\pi^2}{4}J_z^2\sin^2(\pi l) + A^2\frac{J_y - J_x}{4}[J_y - J_x + J_x\cos(\pi h) \\ &+ J_y\cos(\pi k)] + D^2. \end{aligned} \tag{11}$$

In this formula we introduced an empirical anisotropy gap D. The microscopic origin of the D term may be a slight anisotropy of the chain-axis exchange constant (two-ion anisotropy). Near the 1D AF zone center (at large wavelengths), however, these two types of anisotropic contributions cannot be distinguished. It also has to be said that the magnitude of D cannot be independently extracted from the susceptibility measurements that are mostly influenced by yet another spin-

orbit effect, namely the anisotropy of the g factor. The dimensionless mass gap A is given by $A \approx 6.175$.[14]

4. Analysis of inelastic data

In analyzing the b-axis dispersion measured in constant-Q scans, we used the SMA given by Eq. (7), convoluted with the four-dimensional spectrometer resolution function. As we do not have any data for the dispersion along the a axis, to reduce the number of parameters we have assumed $|J_x| = |J_y| = J_\perp$. The relevant adjustable parameters for the fit were thus $J_\perp$, the anisotropy constant D, responsible for the gap at (011), and an intensity prefactor. The chain-axis exchange constant, only needed to take care of resolution effects in the line shape, was fixed to 19.8 meV (see below). The fitting procedure gives $J_\perp = 0.29(2)$ meV and $D = 1.59(4)$ meV. The resulting simulated scans are shown in solid lines in Fig. 5. On the other hand, $J_\perp$ is estimated from the susceptibility data using Eq. (2),[14] which gives $J_\perp = 0.27$ meV for $BaCu_2Si_2O_7$, in excellent agreement with what we find from the analysis of transverse dispersion.

For the dispersion along c, Eq. (9), also convoluted with the four-dimensional spectrometer resolution function, was used to analyze the two measured constant-E scans. Note that at and above 5-meV energy transfer the effect of the anisotropy gap can be neglected. Indeed, the potential energy of magnetic excitations associate with the anisotropy term is expected to add up with their kinetic energy (dispersion) in *squares*, as in Eq. (11). At 5 meV the anisotropy gap is only a 4% effect. Reasonably good fits to the data (solid lines in Fig. 4) were obtained with only three adjustable parameters, namely J_z, an intensity prefactor, and a flat background for each scan. The refined value $J_z = 19.84$ meV is in agreement with the previous estimate based on the experimental $\chi(T)$ curve.

V. CONCLUDING REMARKS

The purpose of this paper was to introduce $BaCu_2Si_2O_7$ as a model $S = 1/2$ quantum antiferromagnet. The particular combination of intrachain and transverse coupling constants make future neutron-scattering studies of this material particularly promising. Indeed, $BaCu_2Si_2O_7$ is a *better* 1D compound than $KCuF_3$ with a smaller ratio of $T_N/J_\parallel$. At the same time the interchain interactions in the silicate are sufficiently strong to make the mass gap easily observable with inelastic neutron-scattering techniques. The use of cold neutrons should enable an experimental study of the double gap, i.e., the separation between the magnon branch and the two-particle continuum. This effect in $BaCu_2Si_2O_7$ is expected be similar to the double gap found in the dimerized state of $CuGeO_3$,[21] but is caused by interchain interactions, rather than dimerization within the chains.

When this work was in progress we became aware of the similar susceptibility data of polycrystalline samples of $BaCu_2Si_2O_7$ and $BaCu_2Ge_2O_7$.[22] These results are consistent with our data.

---

*Present address: Central Research Laboratory, Hitachi Ltd.

[1] M. Hase, I. Terasaki, and K. Uchinokura, Phys. Rev. Lett. **70**, 3651 (1993).

[2] Y. Sasago, M. Hase, K. Uchinokura, M. Tokunaga, and N. Miura, Phys. Rev. B **52**, 3533 (1995).

[3] A. Zheludev, G. Shirane, Y. Sasago, M. Hase, and K. Uchinokura, Phys. Rev. B **53**, 11 642 (1996).

[4] Y. Sasago, K. Uchinokura, A. Zheludev, and G. Shirane, Phys. Rev. B **55**, 8357 (1997).

[5] T. Ami, M. K. Crawford, R. L. Harlow, Z. R. Wang, D. C. Johnston, Q. Huang, and R. W. Erwin, Phys. Rev. B **51**, 5994 (1995).

[6] Z. Hiroi, M. Azuma, and M. Takano, J. Solid State Chem. **95**, 230 (1991).

[7] N. Motoyama, H. Eisaki, and S. Uchida, Phys. Rev. Lett. **76**, 3212 (1996).

[8] Y. Mizuno, T. Tohyama, S. Maekawa, T. Osafune, N. Motoyama, H. Eisaki, and S. Uchida, Phys. Rev. B **57**, 5326 (1998).

[9] J. A. S. Oliveira, Ph.D. thesis, Ruprecht-Karls-Universität, Heidelberg, 1993.

[10] J. C. Bonner and M. E. Fisher, Phys. Rev. **135**, A640 (1964).

[11] To avoid confusion, throughout the paper we will be using the notation for J in which the 1D Hamiltonian is written as $\hat{H} = J\Sigma_i \mathbf{S}_i \cdot \mathbf{S}_{i+1}$.

[12] D. J. Scalapino, Y. Imry, and P. Pincus, Phys. Rev. B **11**, 2042 (1975).

[13] I. Affleck, M. P. Gelfand, and R. R. P. Singh, J. Phys. A **27**, 7313 (1994); **28**, 1787(E) (1995).

[14] H. J. Schulz, Phys. Rev. Lett. **77**, 2790 (1996).

[15] F. H. L. Essler, A. M. Tsvelik, and G. Delfino, Phys. Rev. B **56**, 11 001 (1997).

[16] D. A. Tennant, S. E. Nagler, D. Welz, G. Shirane, and K. Yamada, Phys. Rev. B **52**, 13 381 (1995); D. A. Tennant, R. A. Cowley, S. E. Nagler, and A. M. Tsvelik, *ibid.* **52**, 13 368 (1995).

[17] K. M. Kojima, Y. Fudamoto, M. Larkin, G. M. Luke, J. Merrin, B. Nachumi, Y. J. Uemura, N. Motoyama, H. Eisaki, S. Uchida, K. Yamada, Y. Endoh, S. Hosoya, B. J. Sternlieb, and G. Shirane, Phys. Rev. Lett. **78**, 1787 (1997).

[18] G. Müller, H. Thomas, H. Beck, and J. C. Bonner, Phys. Rev. B **24**, 1429 (1981).

[19] S. E. Nagler, D. A. Tennant, R. A. Cowley, T. G. Perring, and S. K. Satija, Phys. Rev. B **44**, 12 361 (1991).

[20] M. Arai, M. Fujita, M. Motokawa, J. Akimitsu, and S. M. Bennington, Phys. Rev. Lett. **77**, 3649 (1996).

[21] M. Ain, J. E. Lorenzo, L. P. Regnault, G. Dhalenne, A. Revcolevschi, B. Hennion, and Th. Jolicoeur, Phys. Rev. Lett. **78**, 1560 (1997).

[22] T. Yamada and Z. Hiroi (private communication).